THE JOURNAL OF BIOLOGICAL CHEMISTRY
Vol. 273, No. 25, Issue of June 19, pp. 15675–15681, 1998

Printed in U.S.A.

A Revised Model for the Oligomeric State of the *N*-Ethylmaleimide-sensitive Fusion Protein, NSF*

(Received for publication, January 26, 1998)

Karen G. Fleming‡, Tobias M. Hohl§, Richard C. Yu‡, Shirley A. Müller¶, Bettina Wolpensinger¶, Andreas Engel¶, Harald Engelhardt‖, Axel T. Brünger‡, Thomas H. Söllner§, and Phyllis I. Hanson‡‡¶¶**

*From the ‡Department of Molecular Biophysics and Biochemistry, Yale University, New Haven, Connecticut 06520, §Cellular Biochemistry and Biophysics Program, Memorial Sloan-Kettering Cancer Center, New York, New York 10021, ¶Maurice E. Müller Institute at the Biocenter of the University of Basel, CH-4056 Basel, Switzerland, ‖Max-Planck Institute for Biochemistry, Am Klopferspitz 18a, D-82152 Martinsried, Germany, **The Howard Hughes Medical Institute and ‡‡Department of Cell Biology and Physiology, Washington University School of Medicine, St. Louis, Missouri 63110*

The *N*-ethylmaleimide-sensitive fusion protein (NSF) is an ATPase that plays an essential role in intracellular membrane trafficking. Previous reports have concluded that NSF forms either a tetramer or a trimer in solution, and that assembly of the oligomer is essential for efficient activity in membrane transport reactions. However, in recent electron microscopic analyses NSF appears as a hexagonal cylinder similar in size to related ATPases known to be hexamers. We have therefore reevaluated NSF's oligomeric state using a variety of quantitative biophysical techniques. Sedimentation equilibrium and sedimentation velocity analytical ultracentrifugation, transmission electron microscopy with rotational image analysis, scanning transmission electron microscopy, and multiangle light scattering all demonstrate that, in the presence of nucleotide, NSF is predominantly a hexamer. Sedimentation equilibrium results further suggest that the NSF hexamer is held together by oligomerization of its D2 domains. The sedimentation coefficient, $s^0_{20,w}$, of 13.4 (±0.1) S indicates that NSF has unusual hydrodynamic characteristics that cannot be solely explained by its shape. The demonstration that NSF is a hexameric oligomer highlights structural similarities between it and several related ATPases which act by switching the conformational states of their protein substrates in order to activate them for subsequent reactions.

N-Ethylmaleimide-sensitive fusion protein (NSF)[1] is an ATPase that plays an essential role in intracellular membrane trafficking (1). Together with soluble NSF attachment proteins (SNAPs) NSF binds to a group of membrane receptors known as SNAREs (SNAP receptors) which are involved in membrane docking and/or fusion (2). SNAREs are anchored in either donor ("vesicle," v-SNARE) or acceptor ("target," t-SNARE) membranes, and bind to each other to form stable oligomeric complexes (3, 4). NSF and SNAP cooperate to disassemble these SNARE complexes in a reaction that requires ATP hydrolysis; the disassembly is a result of conformational changes that NSF induces in SNAPs and SNAREs (3, 5). Disassembly of SNARE complexes enables individual SNAREs to participate in a dynamic series of protein-protein interactions that are essential for membrane trafficking. The timing of SNARE complex disassembly, and hence of NSF's action relative to the docking and fusion of two membranes has not been definitively established. In different systems, NSF appears to act before membrane docking (6, 7), after membrane docking but before fusion (1, 8), or even after fusion (9).

Nevertheless, it is apparent that inactivation of NSF, either by treatment with *N*-ethylmaleimide or by mutation of residues critical for ATP binding and hydrolysis, leads to accumulation of SNARE complexes and a block in membrane transport reactions (10, 11). To understand the mechanistic details of how ATP hydrolysis-dependent conformational changes within NSF are transduced to SNAPs and SNAREs, an accurate description of NSF's oligomeric structure is essential.

Previous reports have concluded that NSF forms either a tetramer (10) or a trimer (12) in solution, and that assembly of the oligomer is essential for efficient activity in membrane transport reactions (12, 13). Each NSF subunit contains three primary domains: an amino-terminal N-domain required for substrate binding, and two ATPase domains referred to as D1 and D2 required for membrane transport activity and oligomerization, respectively (12, 14, 15). Inactivation of one or more subunits within a single NSF oligomer results in a nonfunctional enzyme, indicating that the NSF oligomer exerts its function through a cooperative mechanism (12).

Recent analyses of NSF's structure by electron microscopy demonstrate that NSF is a hexagonal cylinder (16) similar in size to related ATPases thought to be hexamers in solution (17–20, 34–36). In view of these findings, we have reevaluated NSF's oligomeric structure using a variety of quantitative analytical methods. The results unequivocally show NSF to be a hexamer, held together by oligomerization of its D2 domains.

* This work was supported in part by National Institutes of Health Grants GM16769 (to K. G. F.), GM54160 (to Donald M. Engelman and A. T. B.), and DK2704420 (to James E. Rothman), Swiss National Science Foundation Grant 31-4235.94 (to A. E.), funds from the National Foundation for Cancer Research (to Donald M. Engelman), the Andrew W. Mellon Foundation through a grant to the Tri-Institutional (Cornell/Rockefeller/Memorial Sloan-Kettering) M.D.-Ph.D. program (to T. M. H.), the Maurice E. Müller Foundation, Switzerland (to S. A. M.), and a postdoctoral fellowship from the Helen Hay Whitney Foundation (to P. I. H.). The costs of publication of this article were defrayed in part by the payment of page charges. This article must therefore be hereby marked "*advertisement*" in accordance with 18 U.S.C. Section 1734 solely to indicate this fact.

¶¶ To whom correspondence should be addressed: Dept. of Cell Biology and Physiology, Washington University School of Medicine, 660 S. Euclid, Campus Box 8228, St. Louis, MO 63110. Tel.: 314-747-4233; Fax: 314-362-7463; E-mail: phanson@cellbio.wustl.edu.

[1] The abbreviations used are: NSF, *N*-ethylmaleimide-sensitive factor; SNAP, soluble NSF attachment protein; SNARE, soluble NSF attachment protein receptor; His_6, six-histidine tag; TEM, transmission electron microscopy; STEM, scanning transmission electron microscopy; EM, electron microscopy; ATPγS, adenosine 5′-*O*-(3-thiotriphosphate); DTT, dithiothreitol.

This clearly places NSF among a group of hexameric ATPases with a common mode of action. In many cases they trigger conformational switches in their protein substrates, which in turn engage in subsequent reactions.

EXPERIMENTAL PROCEDURES

Preparation of NSF—NSF bearing an amino-terminal histidine tag and a carboxyl-terminal Myc tag (His_6-NSF-Myc) was expressed in *Escherichia coli* and purified according to published procedures (12, 16). In brief, a bacterial lysate containing His_6-NSF-Myc was incubated with Ni^{2+}-nitrilotriacetic acid agarose (Qiagen) and bound proteins were eluted with imidazole. For sedimentation equilibrium and sedimentation velocity experiments, samples were eluted with steps of imidazole and further purified by size exclusion chromatography on a Superose 6 column (Pharmacia Biotech Inc.) in the indicated final buffers. Peak fractions were stored on ice and used within a few days. For electron microscopy, NSF was eluted with a linear 50–500 mM imidazole gradient. The single symmetric peak was divided into two pools, one containing 90–95% of the NSF (~200–350 mM imidazole, "major peak") and the second containing the trailing 5–10% of the NSF (~350–450 mM imidazole, "trailing edge"). These pools were dialyzed against 20 mM HEPES at pH 7.0, 150 mM KCl, 1 mM $MgCl_2$, 0.5 mM ATP, 1 mM DTT, and 15% (w/v) glycerol (buffer A) or 25 mM HEPES at pH 7.0, 100 mM KCl, 5% (w/v) glycerol, 2 mM $MgCl_2$, 0.5 mM ATP, and 1 mM DTT (buffer B). In some instances His_6-NSF-Myc was purified further on a Superose 6 column run in buffer B. His_6-NSF-Myc was either frozen in liquid N_2 (preparation 1 in Fig. 5*A*) or kept on ice (preparation 2 in Fig. 5*A*) and shipped between laboratories for EM analyses. NSF domain mutant D2 with a carboxyl-terminal His_6 tag was similarly prepared, as described previously (16).

Sedimentation Equilibrium—Equilibrium sedimentation experiments on His_6-NSF-Myc were performed in a Beckman Optima XL-I ultracentrifuge using the interference optics system to visualize the protein. Two sector cells equipped with sapphire windows were used. Blank scans on the buffer were collected at all speeds prior to sedimentation equilibrium experiments. Both blank and sample volumes were 150 μl. Data were collected at 4 °C at speeds of 4700, 5700, 7000, and 8800 rpm on samples at three initial concentrations ranging from 5 to 14 μM in buffer containing 20 mM HEPES at pH 7.6, 150 mM KCl, 5 mM $MgCl_2$, 2 mM β-mercaptoethanol or 5 mM DTT, 1% (v/v) glycerol supplemented with either 1 or 5 mM ATP. Initial protein concentrations were determined by a Bradford protein assay with bovine serum albumin as a standard. Scans were collected at 60 min intervals, and sedimentation equilibrium was established using the MATCH algorithm.

Equilibrium sedimentation data of NSF samples were initially analyzed for average molecular weights in terms of a single, homogeneous species according to

$$c_r = c_m \exp[\sigma(\xi - \xi_m)] + \text{base} \quad \text{(Eq. 1)}$$

where c_r is the concentration of NSF at a given radial position, c_m is the concentration of the enzyme at a reference position (*e.g.* the meniscus), σ is the reduced molecular weight defined as, $\sigma = M(1 - \bar{\nu}\rho)\omega^2/RT$, M is the molecular weight, $\bar{\nu}$ is the partial specific volume, ρ is the solvent density, ω is the angular velocity, $\xi = r^2/2$, r is the radial distance (cm) from the center of rotation, r_m is the radial distance (cm) from the center of rotation to the meniscus, R is the universal gas constant, T is the absolute temperature (Kelvin), and base is a correction term for a non-zero base line. The SEDNTERP program was used to calculate the partial specific volume (0.7348) and the buffer density (1.01142 at 4 °C). The final distribution of species was determined by global fitting of sedimentation equilibrium data according to

$$c_r = c_{m,3} \exp[3\sigma_1(\xi - \xi_m)] + c_{m,6} \exp[6\sigma_1(\xi - \xi_m)] + c_{m,12} \exp[12\sigma_1(\xi - \xi_m)] + \text{base} \quad \text{(Eq. 2)}$$

where σ_1 is the reduced molecular weight defined above) calculated for the NSF monomer and $c_{m,3}$, $c_{m,6}$, and $c_{m,12}$ are the concentrations of the trimeric, hexameric, and dodecameric species at the meniscus. All fits were done by nonlinear least-squares analysis of the primary data using the Windows 95 version of the NONLIN algorithm (21). The fit was optimized by minimization of the variance, and its quality was determined by examination of the residuals.

Equilibrium sedimentation experiments on the D2 fragment of NSF were performed with a Beckman Optima XL-I ultracentrifuge using the absorbance optics system to visualize the protein. Six sector cells equipped with quartz windows were used. The sample volumes were 110 μl. Data were collected at 4 °C at speeds of 10,800, and 13,300 rpm on samples at three initial concentrations ranging from 8 to 20 μM in buffer containing 20 mM HEPES at pH 7.6, 150 mM NaCl, 1 mM $MgCl_2$, 2 mM β-mercaptoethanol, 1% (v/v) glycerol supplemented with 0.2 mM ATP. The best fit distribution of species was described according to

$$c_r = c_{m,6} \exp[\sigma_6(\xi - \xi_m)] + c_{m,12} \exp[2\sigma_6(\xi - \xi_m)] + \text{base} \quad \text{(Eq. 3)}$$

where σ_6 is the reduced molecular weight calculated for the D2 hexamer and the other terms are as described above.

Sedimentation Velocity—Sedimentation velocity data were collected at 4 °C at 24000 or 50000 rpm in 20 mM HEPES at pH 7.6, 150 mM KCl, 5 mM $MgCl_2$, 2 mM β-mercaptoethanol, or 5 mM DTT, 1% (v/v) glycerol using interference optics to visualize the protein. Individual runs were supplemented with 5 mM ADP, 0.5 mM ATP, or 5 mM ATPγS. The sample and buffer volumes were 450 μl. Initial concentrations ranged from 12–230 μg/ml. Scans were collected at the maximum allowed rate of data collection. Data were analyzed according to the time derivative method of Stafford (22–24) using the DCDT software program to yield a sedimentation coefficient distribution, $g(s^*)$, from which a weight average sedimentation coefficient at a particular concentration and temperature can be calculated by integration over the distribution function with respect to s^* as described previously by Stafford (22). The weight average sedimentation coefficient at zero concentration, s^0, was determined by linear extrapolation of the experimental weight average values to infinite dilution. The $s^0_{20,w}$ was calculated from the s^0 value using SEDNTERP.

The time-derivative method of sedimentation velocity analysis can also be used to determine an apparent sedimentation, s_{app}, and an apparent diffusion, D_{app}, coefficient at a particular concentration and temperature by the following relationships (25)

$$D_{app} = (\sigma_{g(s^a)} r_m \omega^2 t)^2/2t \quad \text{(Eq. 4)}$$

where r_m is the radial position of the meniscus (cm), t is the equivalent sedimentation time (seconds), and $\sigma_{s(s^*g)}$ is the standard deviation of the $g(s^*)$ *versus* s^* curve determined by fitting to Equation 5

$$g(s^*) = A \exp[-0.5((s^* - s_{app})/\sigma_{g(s^a)})^2] \quad \text{(Eq. 5)}$$

where A and $\sigma_{s(s^*g)}$ are constants, and s_{app} is the apparent sedimentation coefficient given by the maximum position of the $g(s^*)$ *versus* s^* curve. Values obtained in this manner for s_{app} and D_{app} were used to calculate NSF's mass with the Svedberg equation

$$M = \frac{sRT}{D(1 - \nu p)} \quad \text{(Eq. 6)}$$

where the terms all have their normal meanings.

The NSF frictional coefficient, $f^0_{20,w}$, was calculated from the $s^0_{20,w}$ using an alternate form Svedberg equation (Equation 6) where $D = RT/Nf$. SEDNTERP was used to estimate a value for NSF hydration ($\delta = 0.4071$) from the amino acid composition. Simple interpretation of the frictional coefficient to estimate the NSF axial ratio using an oblate ellipsoid of revolution as a model was also accomplished using SEDNTERP. More complex interpretation of the NSF hydrodynamic shape was accomplished by bead modeling approaches where bead models of the "ATP" and "ADP" forms were created for subsequent analysis using the algorithm HYDRO (26). The beads were arranged so that the mass was distributed according to the size and shape observed for the ADP and ATP forms of NSF by electron microscopy (see Fig. 4*B* in Hanson *et al.* (16)). The mass distribution in the ADP hexagonal ring could be modeled with only 12 beads, whereas the ATP form required 18 beads in order to incorporate the six globular "feet" surrounding the central hexagonal ring. The bead radii used for the ATP and ADP bead models were 20.25 and 23.25 Å, respectively, so that both bead models would have the calculated masses corresponding to an NSF hexamer.

Electron Microscopy—For scanning transmission electron microscopy (STEM), 2–20 μM His_6-NSF-Myc was either stabilized with 0.05% (v/v) glutaraldehyde for 30 min on ice and then diluted to 100–500 nM in buffer A lacking glycerol or directly diluted without the glutaraldehyde step. 3–5-μl aliquots were adsorbed to thin carbon films (supported by thicker perforated carbon layers on gold-coated copper EM grids) which had been rendered hydrophilic by glow discharge in a plasma cleaner. They were subsequently washed on 6 drops of quartz bidistilled water and freeze dried in the STEM HB-5 microscope. Images were recorded at a nominal magnification of 200,000 using doses of 200–400 electrons/nm^2 and an accelerating voltage of 80 kV. Individual particles were manually selected from electron micrographs for mass analysis

and processed as described (28). The beam induced mass loss was determined experimentally by repeatedly scanning the same grid region and monitoring the change in sample mass. The main mass analysis data sets were corrected accordingly (28).

For transmission electron microscopy (TEM) and image processing, 100–250 nM His_6-NSF-Myc (diluted in buffer A lacking glycerol) was absorbed to carbon coated grids which had been rendered hydrophilic as above. The grids were washed once with water and stained with 2% (w/v) uranyl acetate (pH 4.5). Electron micrographs were recorded with a Phillips EM420 at a nominal magnification of 36,000 and an accelerating voltage of 100 kV. The TEM images were digitized in an Eikonix model 1412 camera with a pixel size of 0.43 nm × 0.43 nm at the specimen level. NSF particles were selected from several EM images and subjected to single particle analysis and principle component analysis contained in the SEMPER and EM system program packages (29, 30). The particles were laterally aligned by correlation methods using arbitrary reference molecules and subjected to principal component analysis afterward (31). The first two eigenvectors indicated a significant staining inhomogeneity which resulted in a density gradient across the molecule. Thus, the gradient was substracted prior to a further principal component analysis and classification with respect to eigenvectors representing the symmetry properties of the molecules. A class of 415 particles (out of 1746) was averaged and 6-fold symmetrized.

Size-exclusion Chromatography and Multiangle Laser Light Scattering—Analytical size-exclusion chromatography with multiangle light scattering was performed at 25 °C using a 30 cm × 7.8-mm TSK-Gel G3000SWxl gel filtration column (TosoHaas) at a flow rate of 0.5 ml/min. The column was equilibrated with 20 mM HEPES at pH 7.0, 150 mM NaCl, 4 mM $MgCl_2$, 5 mM DTT, 1% glycerol, and 1 mM ATP. The gel filtration column was followed in-line by a Mini-DAWN light scattering detector (Wyatt Technologies) and an interferometric refractometer (Wyatt Technologies) for protein concentration determination. Molecular weight calculations were carried out using ASTRA software (Wyatt Technologies). The change in refractive index as a function of protein concentration is approximately constant for proteins and a value of 0.193 mol^{-1} was used (27). These experiments were carried out using NSF expressed from a pET15b expression vector (Novagen) from which the NH_2-terminal His_6 tag was removed by thrombin treatment followed by repurification using size exclusion chromatography.

RESULTS AND DISCUSSION

A Hexamer Is the Predominant NSF Species in Solution—Sedimentation equilibrium analytical ultracentrifugation is a thermodynamically rigorous method for characterizing macromolecular mass and oligomeric interactions in solution (32). Analysis of NSF by this method was used to evaluate NSF's oligomeric state in solution. Typical data are shown in Fig. 1. These data, as well as additional data collected at different initial loading concentrations and speeds, were poorly described by a model for a single homogeneous species (Equation 1), and yielded average molecular weights of 483,000–492,000, considerably higher than the 255,000 expected for the previously reported trimeric NSF oligomer (12). The data were then analyzed using models of increasing complexity containing multiple oligomeric species (*e.g.* 1–6, 3–6, 6–12, 4–8, 5–10, 3–6-9, 1–6-12) until global analysis of data collected at different initial concentrations and speeds indicated a best fit model as evaluated by randomness of the residuals and minimization of the variance. As can be seen in Fig. 1, the data collected in 5 mM Mg^{2+}ATP are well described by a distribution containing trimeric, hexameric and dodecameric species (Equation 2), where the hexamer is the predominant species (>90%). Similar results were obtained in buffers containing 1 mM Mg^{2+}ATP, where the best fit model contained monomeric, hexameric and dodecameric species. In all data sets, global fits to sedimentation equilibrium data indicated the predominant species (>90%) to be a hexameric oligomer of NSF. Similar results were independently obtained by sedimentation equilibrium analytical ultracentrifugation with the NSF preparations used for the TEM and STEM analyses shown below.[2]

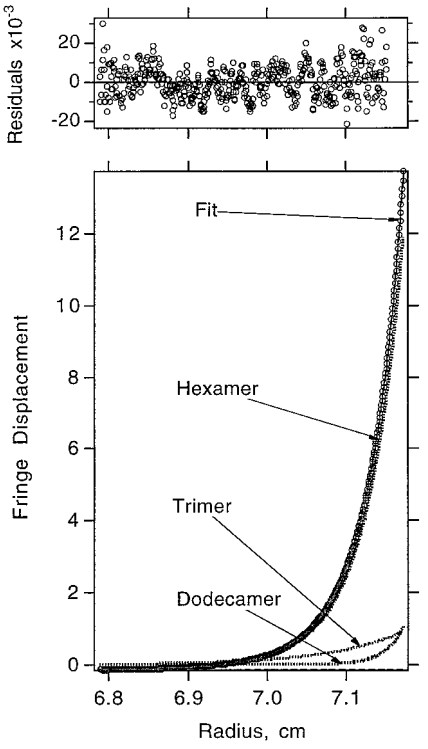

FIG. 1. **Species distribution of oligomeric NSF at sedimentation equilibrium.** The fringe displacement *versus* radius profile for 9 μM NSF in 5 mM Mg^{2+}ATP at 7000 rpm at 4 °C is shown in the *lower panel*. The *open circles* are the data points, and the *solid line* is the model fit described by Equation 2. The three *dotted lines* whose sum gives rise to the fit represent the distributions of trimeric, hexameric, and dodecameric species as indicated. The residuals of the fit to Equation 2 are shown in the *upper panel*.

Attempts to estimate equilibrium constants describing the relationship between the trimeric, hexameric, and dodecameric species from data collected in buffer containing 5 mM Mg^{2+}ATP were unsuccessful, since fits to models containing equilibrium constants showed increased variances as well as systematic deviations in the residuals. This suggests that the hexamer is not in a reversible equilibrium with either the trimeric or dodecameric species on the time scale of the sedimentation equilibrium experiment. Consistent with this conclusion, dilution of NSF samples from the ~10 μM concentration used in these equilibrium centrifugation experiments to ~200 nM in sedimentation velocity experiments (see below) did not change the sedimentation coefficient. Moreover, dilution to ~100–500 nM for electron microscopy (16) (see below) did not change the abundance or appearance of hexameric cylinders. Thus, sedimentation equilibrium shows NSF to be a stable hexamer, not trimer, in solution.

The D2 Fragment of NSF Is an Oligomerization Domain—Each 85-kDa NSF subunit consists of three primary domains termed N, D1, and D2 (14, 15). Electron microscopy of the D1-D2 and the D2 domains showed ring-shaped structures similar to those formed by full-length NSF (16). Since the D2 domain appears to be essential for NSF's oligomerization (12, 39) we examined its oligomeric state by sedimentation equilibrium which yielded the data shown in Fig. 2. In buffer containing 0.2 mM Mg^{2+}ATP, the predominant species in solution is a D2 hexamer. The presence of ATP appears to be essential for hexamer formation and/or stabilization, since these hexamers were destabilized in samples from which ATP had been removed by gel filtration (data not shown). The present findings are thus consistent with earlier studies demonstrating oligomerization of the D2 domain (12, 16, 39) and confirm a direct role of both ATP binding to the D2 domain and of this domain's

[2] R. Jaenicke and A. Lustig, personal communication.

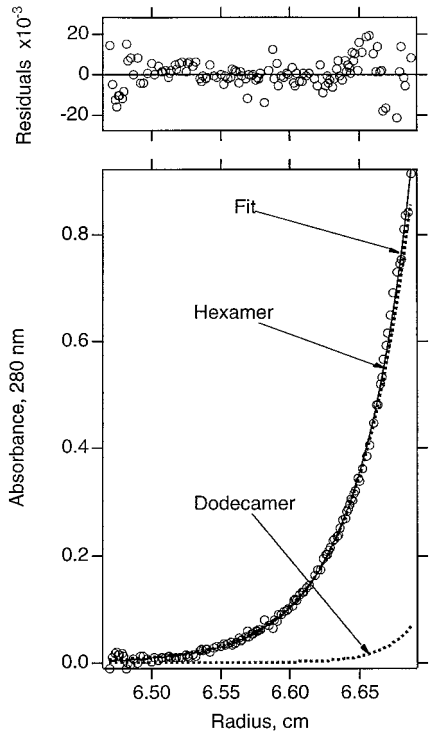

FIG. 2. **Species distribution of oligomeric D2 fragment of NSF at sedimentation equilibrium.** The absorbance *versus* radius profile for 10 μM D2 fragment in 0.2 mM Mg^{2+}ATP at 13,300 rpm at 4 °C is shown in the *lower panel*. The *open circles* are the data points, and the *solid line* is the model fit described by Equation 3. The two *dotted lines* whose sum gives rise to the fit represent the distributions of hexameric and dodecameric species as indicated. The residuals of the fit to Equation 3 are shown in the *upper panel*.

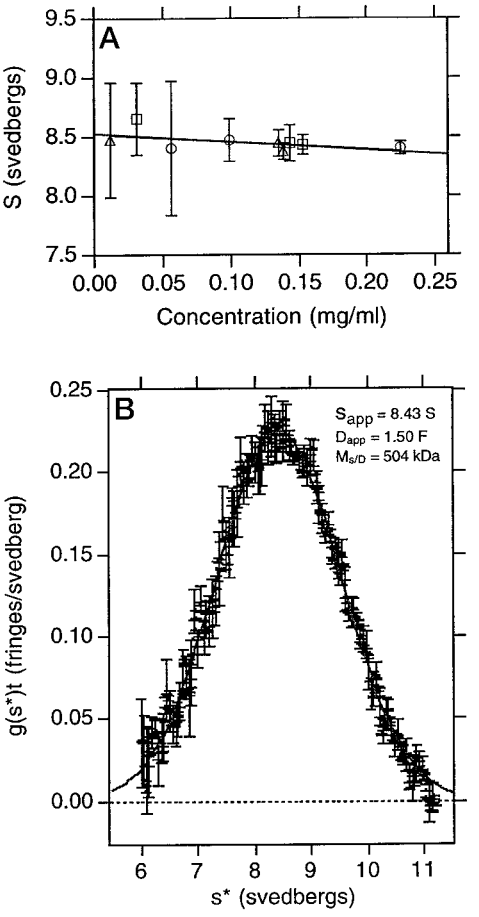

FIG. 3. **Sedimentation velocity analysis of NSF.** *Panel A* shows the apparent weight average sedimentation coefficients in the presence of 5 mM $MgCl_2$ with either 0.5 mM ATP (*open squares*), 5 mM ATPγS (*open triangles*), or 5 mM ADP (*open circles*) as a function of total protein concentration. Extrapolated to infinite dilution, the sedimentation coefficients for NSF in these three conditions are all consistent with an s^0 value of 8.52 at 4 °C in buffer. This corrects to an $s^0_{20,w}$ of 13.4 at 20 °C in water. *Panel B* shows the apparent sedimentation coefficient distribution function, $g(s^*)$ *versus* s^*, for 0.23 mg/ml NSF in buffer containing 5 mM Mg^{2+}ADP collected at 24,000 rpm at 4 °C. The *error bars* represent the standard error of the mean of the 10 data sets used in this analysis. For clarity, only every fifth error bar is shown. The *solid line* is the fit to Equation 5. Apparent s, D, and $M_{s/D}$ values were calculated as described in the text.

oligomerization in organizing NSF's hexameric structure.

Sedimentation Velocity Experiments Reveal an Unusual Hydrodynamic Property of NSF—The observation that hexameric NSF is the predominant species in solution does not agree with previous sedimentation equilibrium studies in which NSF was shown to be trimeric (12). In both studies, however, the same protein construct (His_6-NSF-Myc) and similar purification steps were used. In an effort to compare the NSF samples evaluated in this study with the material analyzed in previous studies, the sedimentation coefficient of NSF was measured by velocity sedimentation analytical ultracentrifugation. All experiments yielded data described by a $s^0_{20,w}$ of 13.4 ($\pm$0.1) S, regardless of whether Mg^{2+}ADP, Mg^{2+}ATP, or Mg^{2+}ATPγS was included in the buffer (see Fig. 3*A*). This sedimentation coefficient is consistent with the previously reported value of 12.9 S as well as with the analysis of NSF's sedimentation relative to standards through glycerol gradients (12, 19).

A sedimentation coefficient of 13.4 S is low for a 510-kDa protein (the hexameric molecular mass of His_6-NSF-Myc) considering that the predicted s_{max} values for a spherical protein of equivalent mass and partial specific volume would be 20.1 S (anhydrous) and 18.5 S (hydrated, where $\delta = 0.4071$, calculated from NSF's amino acid composition). Such a low sedimentation coefficient suggests that NSF's frictional coefficient may be unusually high. Electron microscopy indicated that NSF consists of a $\sim$13 $\times$ 10-nm hollow cylinder with a larger surface area and increased subunit flexibility relative to that expected for a sphere of the same mass and density (16) (Fig. 4). This difference in size and shape would indeed be expected to increase the frictional coefficient and decrease the sedimentation coefficient.

To determine whether the hexagonal ring shape could explain the low sedimentation coefficient, we constructed several simple models for NSF's shape and defined their hydrodynamic properties using HYDRO (26). The models were built using the minimum number of beads required to form the hexagonal

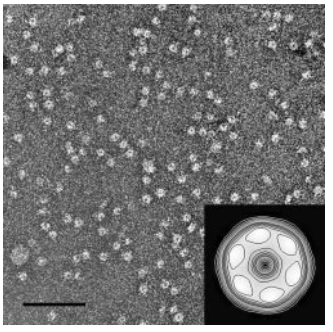

FIG. 4. **Electron microscopy and average of NSF.** Survey view of negatively stained NSF particles prepared in the presence of Mg^{2+}ATP. The *inset* shows the 6-fold symmetrized average of 415 top view projections. The diameter of the ATPase is 13 nm. Six protein regions surrounding a central electron-dense region, indicative of a stain-filled channel or cavity (diameter 2–3 nm), are clearly recognizable. *Scale bar* = 100 nm.

A

Sample Preparation	Fraction	Fixation	Final [Protein] nM	Particle Mass ± SD, kDa	Number of Particles (n)
1	trailing edge	no	160	471 ± 90	335
1	trailing edge	yes	120	488 ± 77	1613
2	main peak	yes	200	459 ± 96	1508
2	main peak + gel filtration	yes	160	497 ± 90	906
2	trailing edge	yes	150	467 ± 84	1083
2	trailing edge	yes	470	494 ± 81	713

B

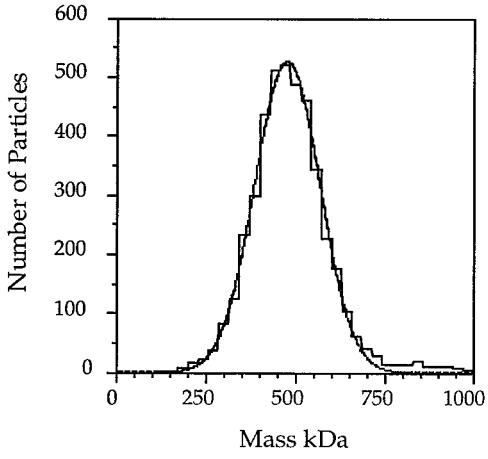

FIG. 5. **STEM mass determination of NSF.** Results of STEM mass determinations utilizing two preparations and different fractions of His_6-NSF-Myc eluting from a Ni^{2+}-NTA column (see "Experimental Procedures") are listed in *A* with the corresponding molecular masses, standard deviations (*SD*), and number of particles in the histogram peak (*n*). *Preparation 1*, stored frozen at −80 °C; *preparation 2*, stored on ice. The data have been corrected for the ~4% beam induced mass loss incurred during measurement. Pooled mass data sets from the individual experiments made with NSF preparation 2, after individual correction for beam induced mass loss, are displayed as a histogram in *B*. The Gaussian fit indicates a mass of 475 ± 91 kDa (n = 4262), consistent with the presence of hexameric NSF oligomers. There is no shoulder or peak in the 200–300-kDa region of the histogram, which would be the mass region of NSF trimers.

structures observed in EM images of NSF oligomers either in Mg^{2+}ATPγS or in Mg^{2+}ADP (16) and are described in detail under "Experimental Procedures." Although the S value predicted for the ATP bead model (13.8 S, where δ = 0.4071) agrees fairly well with the experimental sedimentation coefficient (13.4 S), the value predicted for the ADP bead model (15.9 S, where δ = 0.4071) is too high and can only approximate the experimental S value if δ = 0.9–1.2, an unusually high value for hydration. Thus, although the sedimentation coefficient is significantly reduced by NSF's hexagonal ring shape, the shape *alone* cannot explain the abnormally low S value as long as standard estimates of hydration are assumed. Additional experimentation, such as small angle x-ray scattering, will be required to further evaluate NSF's structure in solution.

Sedimentation velocity analysis can be extended using a time-derivative method which provides a means to simultaneously determine the apparent sedimentation, s_{app}, and diffusion, D_{app}, coefficients, from which the molecular weight can be calculated (25) (see "Experimental Procedures"). Even though both coefficients are hydrodynamic measures of a macromolecule, the ratio s/D is proportional to the molecular weight by the Svedberg equation where the hydrodynamic shape and hydration factors inherent in each coefficient cancel. Fig. 3*B* shows such an analysis of NSF sedimentation velocity data collected in 5 mM Mg^{2+}ADP. Using Equations 4 and 5 we calculated an s_{app} of 8.43 S and a D_{app} of 1.50 Ficks. When combined in the Svedberg equation, these yielded a solution molecular mass of 504 kDa. This value is within 2% of NSF's calculated hexameric molecular mass.

TEM and Image Processing Demonstrate that NSF Is a Hexagonal Cylinder with 6-fold Symmetry—Recent quick-freeze/deep-etch EM showed that NSF and its domain mutants have dimensions and a 6-fold symmetry consistent with a hexagonal, and therefore possibly hexameric, structure (16). Analysis of negatively stained NSF oligomers by TEM and image processing (Fig. 4) was used to confirm this 6-fold symmetry. Top view projections of NSF prepared in 1 mM Mg^{2+}ATP were aligned and subjected to principle component analysis (see "Experimental Procedures" for details). The molecules were classified using the most significant eigenvectors which represented the symmetry properties of the particles. The averages obtained from these particles demonstrated an apparent 6-fold symmetry which was enhanced by rotational symmetrization (Fig. 4, *inset*). According to this average, negatively stained NSF oligomers had a diameter of ~13 nm, consistent with a previously reported measurement (33) and with measurements of platinum-shadowed NSF after substracting the ~2-nm platinum coating (16). The TEM images also show NSF to contain a central electron-dense region with a diameter of 2–3 nm representing a stain-filled pore or cavity (Fig. 4).

Quantitative STEM Analysis of NSF Particles Reveals a Mass Consistent with a Hexameric Structure—STEM mass analysis of unstained, freeze-dried NSF particles confirmed a hexameric structure. This technique enables mass measurements of individual macromolecules that are independent of their hydrodynamic properties (10, 11). All experiments with NSF (His_6-NSF-Myc preparations 1 and 2) yielded mass histograms which exhibited a Gaussian distribution with a single

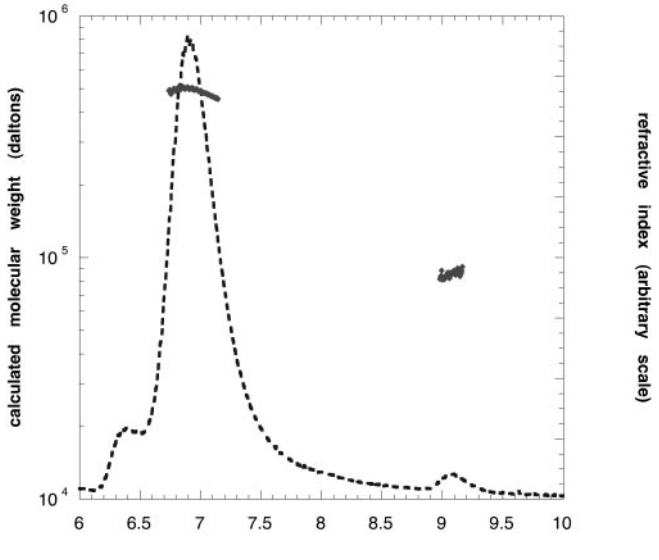

FIG. 6. **Multiangle light scattering of NSF.** A typical elution profile is shown in buffer supplemented with 1 mM Mg^{2+}ATP. The *dotted line* represents refractive index on an arbitrary scale, which is proportional to protein concentration, and *diamonds* indicate calculated molecular mass. The molecular mass profile across the peak at 7 ml reflects a 489 (±5)-kDa, hexameric NSF; the peak at 9.1 ml reflects an 85 (±3)-kDa monomeric NSF.

well defined peak at 459–497 kDa (Fig. 5*A*; histograms not shown), consistent with the presence of a hexamer. There was no detectable shoulder or peak in the 200–300 kDa region of the histograms which would have indicated the presence of significant amounts of a stable NSF trimer. In addition, a series of experiments allowed us to examine the effects of chemical cross-linking and freeze-thawing on NSF's oligomeric state. Comparison of NSF samples prepared and treated in different ways (Fig. 5*A*) showed that glutaraldehyde stabilization, freeze-thawing, and additional purification did not significantly alter the measured mass. Within experimental variability, all experiments gave equivalent results showing the presence and predominance of the NSF hexamer. Pooling the data from all experiments using one NSF preparation (preparation 2) yielded the histogram shown in Fig. 5*B*, with a mass for NSF of 475 ± 91 kDa (n = 4262).

Multiangle Light Scattering and Gel Filtration Support the Hexameric Structure in Solution—The finding that NSF is predominantly a hexamer in solution was further supported by multiangle light-scattering experiments. This technique offers an additional shape-independent approach for the determination of molecular mass (38). Most NSF elutes from size-exclusion columns slightly ahead of the 440-kDa ferritin standard, implying a molecular mass consistent with a hexameric state (16). Fig. 6 shows a typical gel-filtration elution profile of NSF together with an in-line multiangle light-scattering molecular mass determination. The predominant NSF species, averaged across the peak center (width at half height), is calculated by multiangle light scattering to be 489 (± 5) kDa. This value corresponds well to the predicted hexameric molecular mass of 510 kDa. A smaller peak eluting later consists of an 85 (± 3)-kDa species, which corresponds to monomeric NSF. Distinct peaks of other possible NSF oligomers are not observed in 1 mM Mg^{2+}ATP. Since the NSF used in these experiments had its amino-terminal His_6 tag removed (see "Experimental Procedures"), this result also rules out the unlikely possibility that the His_6 tag itself is responsible for NSF's hexameric oligomeric state.

Conclusions—Analytical ultracentrifugation, transmission electron microscopy with image processing, scanning transmission electron microscopy, and dynamic light scattering all reveal that NSF is a hexamer. This result differs from previously published experiments which suggested that NSF was a trimer (12). It remains unclear why the prior sedimentation equilibrium experiments are not consistent with the current data. The sedimentation equilibrium experiments described here were confirmed in three independent laboratories with equivalent results, supporting a hexameric structure (Fig. 1).[2] Additional evidence for the previously proposed trimeric structure was provided by the presence of dimeric and trimeric products in cross-linking experiments (12). However, several factors including inefficient cross-linking, low sensitivity of Coomassie staining, and exclusion of high molecular weight complexes from the SDS-polyacrylamide gels used for analysis could have prevented the detection of higher order oligomers (tetramers, pentamers, and hexamers).

The possible limitations of each technique employed in the present study were addressed by comparing the results from a variety of approaches that are based on different physical principles and measure different parameters of the oligomer's behavior. In particular, the range of methods chosen allowed NSF's oligomeric size to be determined in manners both dependent on, and independent of, its shape and hydrodynamic properties, using protein in solution as well as protein that had been attached to a solid support. The measurements, which were carried out over a wide concentration range and in different buffers, always lead to the same conclusion, NSF is genuinely a hexamer.

Interestingly, the sedimentation coefficient of NSF ($s^0_{20,w}$ of 13.4 (±0.1) S) closely matches the low value reported previously (12), suggesting that this oligomer has a large frictional coefficient for its size and shape. Further studies will be required to establish whether this is a result of hydration or conformational flexibility of the oligomers in solution, perhaps corresponding to the conformational changes seen in the presence of different nucleotides by quick-freeze/deep-etch electron microscopy (16).

The similarity between NSF, p97, CDC48, and other related ATPases including the Hsp100 proteins ClpA and Hsp104 thus extends to their basic structural design of six identical subunits per cylindrical oligomer (16–20, 34–36). This arrangement is likely to play a role in the mechanism by which these ATPases interact with and affect the conformation of their target substrates.

Acknowledgments—The MATCH algorithm and the NONLIN software were provided by the University of Connecticut Biotechnology Center (Storrs, CT). SEDNTERP was developed by J. Philo, D. Hayes and T. M. Laue. The DCDT program was provided by W. F. Stafford III. All four of these software programs are available from the RASMB homepage at http://www.bbri.harvard.edu/rasmb/rasmb.html. We thank Donald M. Engelman, John Heuser, Reinhard Jahn, James E. Rothman, Walter F. Stafford III, Olwyn Byron, and Wolfgang Baumeister for important input and helpful conversations. We thank Rainer Jaenicke and Ariel Lustig for independently confirming the ultracentrifugation results on the TEM and STEM samples as well as for critical reading of the manuscript. We thank Susanne Volker-Mürkl for technical assistance.

REFERENCES

1. Rothman, J. E. (1994) *Nature* **372,** 55–63
2. Söllner, T., Whiteheart, S. W., Brunner, M., Erdjument-Bromage, H., Geromanos, S., Tempst, P., and Rothman, J. E. (1993) *Nature* **362,** 318–324
3. Söllner, T., Bennett, M. K., Whiteheart, S. W., Scheller, R. H., and Rothman, J. E. (1993) *Cell* **75,** 409–418
4. Hayashi, T., McMahon, H., Yamasaki, S., Binz, T., Hata, Y., Südhof, T. C., and Niemann, H. (1994) *EMBO J.* **13,** 5051–5061
5. Hanson, P. I., Otto, H., Barton, N., and Jahn, R. (1995) *J. Biol. Chem.* **270,** 16955–16961
6. Mayer, A., Wickner, W., and Haas, A. (1996) *Cell* **85,** 83–94
7. Nichols, B. J., Ungermann, C., Pelham, H. R. B., Wickner, W. T., and Haas, A. (1997) *Nature* **387,** 199–202

8. Banerjee, A., Barry, V. A., DasGupta, B. R., and Martin, T. F. J. (1996) *J. Biol. Chem.* **271,** 20223–20226
9. Boudier, J., Charvin, N., Boudier, J., Fathallah, M., Tagaya, M., Takahashi, M., and Seagar, M. J. (1996) *Eur. J. Neurosci.* **8,** 545–552
10. Block, M. R., Glick, B. S., Wilcox, C. A., Wieland, F. T., and Rothman, J. E. (1988) *Proc. Natl. Acad. Sci. U. S. A.* **85,** 7852–7856
11. Søgaard, M., Tani, K., Ye, R. R., Geromanos, S., Tempst, P., Kirchhausen, T., Rothman, J. E., and Söllner, T. (1994) *Cell* **78,** 937–948
12. Whiteheart, S. W., Rossnagel, K., Buhrow, S. A., Brunner, M., Jaenicke, R., and Rothman, J. E. (1994) *J. Cell Biol.* **126,** 945–954
13. Nagiec, E. E., Bernstein, A., and Whiteheart, S. W. (1995) *J. Biol. Chem.* **270,** 29182–29188
14. Wilson, D. W., Wilcox, C. A., Flynn, G. C., Chen, E., Kuang, W. J., Henzel, W. J., Block, M. R., Ullrich, A., and Rothman, J. E. (1989) *Nature* **339,** 355–359
15. Tagaya, M., Wilson, D. W., Brunner, M., Arango, N., and Rothman, J. E. (1993) *J. Biol. Chem.* **268,** 2662–2666
16. Hanson, P. I., Roth, R., Morisaki, H., Jahn, R., and Heuser, J. E. (1997) *Cell* **90,** 523–535
17. Peters, J.-M., Harris, J. R., Lustig, A., Müller, S., Engel, A., Volker, S., and Franke, W. W. (1992) *J. Mol. Biol.* **223,** 557–571
18. Parsell, D. A., Kowal, A. S., and Lindquist, S. (1994) *J. Biol. Chem.* **269,** 4480–4487
19. Kessel, M., Maurizi, M. R., Kim, B., Kocsis, E., Trus, B. L., Singh, S. K., and Steven, A. C. (1995) *J. Mol. Biol.* **250,** 587–594
20. Beyer, A. (1997) *Protein Sci.* **6,** 2043–2058
21. Johnson, M. L., Correia, J. J., Yphantis, D. A., and Halvorson, H. R. (1981) *Biophys. J.* **36,** 575–588
22. Stafford, W. F., III (1992) *Anal. Biochem.* **203,** 295–391
23. Stafford, W. F., III (1994) in *Modern Analytical Ultracentrifugation* (Schuster, T., and Laue, T. M., eds), pp. 119–137, Birkhauser, Boston
24. Stafford, W. F., III (1994) *Methods Enzymol.* **240,** 478–501
25. Stafford, W. F., III (1996) *Biophys. J.* **70,** M-Pos452
26. Garcia de la Torre, J., Navarro, S., Lopez Martinez, M. C., Diaz, F. G., and Lopez Cascales, J. J. (1994) *Biophys. J.* **67,** 530–531
27. Wen, J., Arakawa, T., and Philo, J. S. (1996) *Anal. Biochem.* **240,** 155–166
28. Müller, S. A., Goldie, K. N., Bürki, R., Häring, R., and Engel, A. (1992) *Ultramicroscopy* **46,** 317–334
29. Hegerl, R. (1996) *J. Struct. Biol.* **116,** 30–34
30. Saxton, W. O. (1996) *J. Struct. Biol.* **116,** 230–236
31. Frank, J., and van Heel, F. J. (1982) *J. Mol. Biol.* **161,** 134–137
32. Hensley, P. (1996) *Structure* **4,** 367–373
33. Whiteheart, S. W., and Kubalek, E. W. (1995) *Trends Cell Biol.* **5,** 64–68
34. Fröhlich, K., Fries, H., Peters, J. M., and Mecke, D. (1995) *Biochim. Biophys. Acta* **1253,** 25–32
35. Pamnani, V., Tamura, T., Lupas, A., Peters, J., Cejka, Z., Ashraf, W., and Baumeister, W. (1997) *FEBS Lett.* **404,** 263–268
36. Zhang, L., Ashendel, C. L., Becker, G. W., and Morre, D. J. (1994) *J. Cell Biol.* **127,** 1871–1883
37. Engel, A. (1978) *Ultramicroscopy* **3,** 273–281
38. Wyatt, P. (1993) *Anal. Chim. Acta* **272,** 1–40
39. Matveeva, E. A., He, P., and Whiteheart, S. W. (1997) *J. Biol. Chem.* **272,** 26413–26418